Exploring x-ray irradiation conditions for triggering ultrafast diamond graphitization

Vladimir Lipp [*]

Center for Free-Electron Laser Science CFEL, Deutsches Elektronen-Synchrotron DESY, Notkestr. 85, 22607 Hamburg, Germany

Victor Tkachenko

European XFEL, Holzkoppel 4, 22869 Schenefeld
and Center for Free-Electron Laser Science CFEL, Deutsches Elektronen-Synchrotron DESY, Notkestr. 85, 22607 Hamburg, Germany

Ichiro Inoue

RIKEN SPring-8 Center, 1-1-1 Kouto, Sayo 679-5148, Hyogo, Japan

Philip Heimann

Linac Coherent Light Source, SLAC National Accelerator Laboratory, 2575 Sand Hill Road, Menlo Park, California 94025, USA

Anastasiia Ryzhkova

Taras Shevchenko National University of Kyiv, 64/13, Volodymyrska Street, 01601 City of Kyiv, Ukraine

Abdelkhalek Bashandi

Department of Physics, Faculty of Science, Cairo University, 1 Gamaa Street, 12613 Giza, Egypt

Beata Ziaja [†]

Center for Free-Electron Laser Science CFEL, Deutsches Elektronen-Synchrotron DESY, Notkestr. 85, 22607 Hamburg, Germany
and Institute of Nuclear Physics, Polish Academy of Sciences, Radzikowskiego 152, 31-342 Kraków, Poland

Intense femtosecond x-ray pulses produced by an x-ray free-electron laser can trigger irreversible structural transitions in crystalline solids. For instance, irradiation of diamond can lead to graphitization and, at higher deposited doses, to amorphization. Our Monte Carlo simulations of irradiated diamond under realistic experimental conditions demonstrate that triggering graphitization or other phase transitions with hard x-ray photons can be challenging due to the ballistic escape of photoelectrons out of the beam focus. The decisive parameter here is the photoelectron range in proportion to the focal beam size. For future experiments on x-ray-induced transitions, such dedicated simulations of ballistic transport preceding the beamtime will be necessary. They can predict experimental conditions under which the desired distribution of the absorbed x-ray dose in the irradiated solid can be achieved.

I. INTRODUCTION

Femtosecond x-ray pulses produced by the modern x-ray free-electron lasers (XFELs) [1–5] can be sufficiently intense to cause irreversible structural damage to crystalline solids, including radiation-hard diamond [6–8].

Within the first hundred femtoseconds after an absorption of an x-ray pulse, the electron subsystem in an irradiated solid undergoes a strongly nonequilibrium evolution triggered by the so-called electron cascading [9–11]. In case of hard x-rays, energetic photo-, Auger, and secondary electrons inelastically scatter on the target atoms, creating an avalanche of excited secondary electrons. On the ultrafast timescales considered, the excited electrons propagate ballistically [12], in contrast to a slow diffusive motion of low-energy conduction-band electrons. The electron cascading finishes when all the cascade electrons lose most of their energy on impact ionizations and can no longer excite secondary electrons. The resulting distribution of low-energy excited electrons in the conduction band may affect the atomic potential energy surface and lead to a nonthermal transition, such as disordering [8,13] or graphitization [14], on femtosecond timescales. This occurs when a sufficient number of electrons is excited in the conduction band [15–19].

According to experimental and theoretical studies in Refs. [6,14], diamond irradiated with extreme ultraviolet (XUV) pulse undergoes graphitization on a timescale of about 150 fs, if the absorbed dose reaches about 1 eV/atom (see also the update of the dose value in Ref. [20]). It is to be emphasized that the final state of the material after this time is an

---

[*]Contact author: vladimir.lipp@desy.de
[†]Contact author: beata.ziaja-motyka@cfel.de

024103-1

overdense graphite [19], i.e., only sp3 → sp2 rebonding takes place during 150 fs. Another simulation performed with a hybrid Monte Carlo/density functional tight binding/molecular dynamics tool XTANT+ indicated that the graphitization threshold is about 2 eV/atom and only a partial graphitization can be expected on a timescale of about 500 fs [20].

However, in a more recent work by Heimann *et al.* [8], the attempt to directly observe graphitization on femtosecond time scales, induced by hard x-rays, was unsuccessful. Diamond disordering was observed instead. Also in the recent work by Lütgert *et al.* [21], the authors found no evidence of the diamond graphitization caused by the heavy ion beam at a similar dose deposition.

In this work, we perform dedicated Monte Carlo simulations with the XCASCADE-3D code, in order to investigate the effect of ballistic electron transport on the hard x-ray-induced ultrafast structural transformations in diamond. The irradiation parameters are taken from the recent experimental work [8]. We show that the ballistic electron motion can result in a strongly nonuniform spatial redistribution of the transient number of low-energy conduction-band electrons in the irradiated crystal. According to earlier studies, a sufficient number of such electrons is needed to initiate the graphitization process [14,20,22]. The escape of the electrons out of the beam focus can yield effective absorbed x-ray doses much lower than those expected after assuming a full absorption of the pulse within the lateral beam focus. This shows that dedicated simulations, preceding planned graphitization, and other phase-transition experiments induced by x-rays, may be necessary in order to establish proper irradiation conditions needed for such experiments.

II. EXPERIMENTAL PARAMETERS

Parameters of the present simulations correspond to the recently published experimental study on the nonthermal structural transformation in diamond performed at the SACLA XFEL facility [8]. In that study, a nanocrystalline diamond layer with the thickness of $L = 20$ μm was irradiated with a 6 fs x-ray pulse. XFEL photon energy was 7 keV. At SACLA, the beam profiles can be well described by a Gaussian function [23–26]. Various pulse energies E_{beam}, spot areas S, and, consequently, different volumetric nominal absorbed doses D, were applied. The dose is defined as

$$D = E_{beam} \times (1 - \exp(-L/\lambda_{att})) \frac{1}{n_a L \times S}, \quad (1)$$

where $n_a = 176$ nm^{-3} is the average atomic number density for diamond under ambient conditions.

In the experiment [8], the diamond x-ray pump-probe analysis included several data sets. They were combined into three groups as shown in Table I. The foci are defined as full width at half maximum (FWHM) spots.

III. MODEL

Simulations presented in this work have been performed using our in-house classical Monte Carlo code XCASCADE-3D [27], which was first introduced in Ref. [28]. Later, it was used to explain a number of experimental observations in

TABLE I. Irradiation parameters used in Ref. [8] combined into three data sets.

Experimental group	D (eV/atom)	Focus (μm^2)	E_{beam} (μJ)	Calculated peak electron density (%)
1.1	1.3	1.83×1.15	33	1.6
1.2	1.4	1.44×1.10	27	1.7
1.3	1.5	1.06×1.05	21	1.8
1.4	1.5	0.92×0.86	15	1.7
2.1	5.2	0.78×0.66	33	5.5
2.2	5.7	0.59×0.51	21	5.0
2.3	8.7	0.40×0.35	15	5.9
3.1	16	0.40×0.35	27	10
3.2	54	0.14×0.16	15	12

ultrafast x-ray science, such as damage to ruthenium mirrors induced by XUV light and hard x-rays [29], or transient optical properties of irradiated Si_3N_4 [30]. The tool also enabled us to identify suitable materials or pulse parameters in various x-ray-related applications [12].

The XCASCADE-3D simulation tool can provide temporal and spatial characteristics of x-ray-induced electron cascades in various solids on femtosecond time scales. In particular, the code resolves fast electron ballistic transport, which affects the distribution of the x-ray dose absorbed. In order to describe photoabsorption and electron scattering on atoms, the code uses an atomistic approximation: it applies atomic cross sections (for isolated atoms and ions) and atomic ionization potentials. They are extracted from the EPICS 2017 database [31]. Decay of the created deep-shell holes is simulated by taking into account the characteristic Auger decay times from Ref. [32]. More details can be found in Ref. [12].

The XCASCADE-3D results presented here were averaged over up to one million Monte Carlo realizations to achieve reliable statistics. The grid size for the figures was 10 nm × 10 nm × 10 nm. The beam propagation axis was chosen to be parallel to the z axis (directed in depth into the material) both in the simulations and in the plots. The x-ray polarization was linear and parallel to the x axis. In the present simulations, similarly to Ref. [29], it was taken into account by assuming that a half of the photoelectrons started their motion in the direction $+X$, and the other half did in the direction $-X$. In reality, a cosine angular distribution is expected [33] [Eq. (3.29) therein], i.e., we somewhat overestimate the effect of the electron spread with our simplifying assumption. The anisotropic, cosine photoelectron distribution will be implemented into a future version of the software. The photoelectrons underwent elastic and inelastic scatterings, leading to the creation of Auger and secondary electrons, until their energy fell below the lowest ionization threshold for diamond. According to the EPICS database [31], the ionization threshold for a carbon atom in diamond is 11.26 eV. In our simulations, when the energy of a high-energy electron decreases below this value, we assume that the electron stops its motion and becomes an excited electron in the conduction band. To justify this assumption, we estimated the progress of diffusive motion for electrons with the energy of ~11 eV as 4.35 A/fs$^{0.5}$, which means that such electrons only travel a distance of ~6 nm

within 200 fs. This diffusion distance is very small compared with the photoelectron range, which is about 312 nm at the simulated photon energy [12].

Since the goal of this work is to study possible diamond graphitization caused by low-energy excited electrons in the conduction band, we do not include electrons with energies above 11.26 eV into the plots, assuming that they do not affect the potential energy surface, i.e., they do not trigger graphitization.

In order to take into account experimental x-ray spot sizes, in this work we implemented a dedicated convolution procedure, which assumes that each electron cascade starts at the site of a photoabsorption and evolves independently. The spatial distributions of the absorbed photons along x and y axes are Gaussian. The distribution of absorbed x-ray energy along the z axis is assumed to be homogeneous, due to the large x-ray attenuation length. Namely, for the experimental photon energy, 7 keV, the corresponding photon attenuation length is, $\lambda_{att} = 428$ μm [34]. The simulation volume is then a layer of a certain thickness (less than photon attenuation length), infinite in x and y. Here, it has a thickness of $L = 20$ μm, as in the experiment [8].

According to the XCASCADE-3D simulations, the electron cascading time for 7 keV photon in diamond is about 14 fs [12]. This means that 14 fs after a photoabsorption event, a majority of the excited electrons stop their motion and join the low-energy fraction of conduction-band electrons.

A typical calculation for each set of beam parameters takes about two hours on Intel(R) Xeon(R) W-2225 CPU @ 4.10GHz, using 8 CPU cores.

IV. RESULTS

In Fig. 1, we present selected distributions of the electron density in diamond predicted at the temporal maximum of the pulse intensity, $t = 0$ fs, with the abovementioned parameters. Figures 1(a)–1(f) represent selected experimental cases (1,1), (1,2), (2,1), (2,3), (3,1), and (3,2), respectively. Solid red (green) curves show transient electron density along the x (y) axis, which is parallel (perpendicular) to the beam polarization. Beam propagates along the z axis both in the simulations and in the plots. Dashed (dot-dashed) lines represent the simulated distribution of the absorbed photons [calculated also along the x (y) axis] multiplied by the average number of electrons per a single 7 keV photon in diamond at $t = 0$ fs (∼45.6). In other words, these curves correspond to a simulation not accounting for the electron transport, which effectively means that they reflect the original x-ray spatial profile. We will call these predictions "nontransport" ones.

The XCASCADE-3D predictions demonstrate how the electron transport affects the spatial distribution of excited electrons. For example, for the wide (micrometer) focusing, Figs. 1(a) and 1(b), the transport and nontransport electron distributions coincide with each other, suggesting that the electron ballistic transport could be neglected under these conditions. In contrast, in Fig. 1(f), the electron distributions along the x axis and y axis strongly differ from the respective nontransport ones, indicating that the electron transport does play a significant role in case of tight focusing. The electron density along x spreads significantly wider than that along

the y axis. This is expected, due to the x-ray polarization directed along the x axis. Similar behavior can be observed in Figs. 1(c)–1(e) at (still) submicrometer focusing.

The observations can be explained in the following way. As we mentioned earlier, the electron range under the considered conditions is about 312 nm. The larger the beam spot is, the lower is the effect of the ballistic electron transport on the spatial redistribution of the absorbed x-ray energy. For the beam spots much larger than the electron range, the respective effect of electron transport becomes negligible.

Figure 2 shows the electron density distributions at 30 fs, when electron cascading was finished. As we mentioned earlier, the duration of the latter is about 14 fs. Taking into account the pulse duration of 6 fs, one can expect no ballistic transport after 20–30 fs. As in Fig. 1, dashed (dot-dashed) lines represent the simulated distribution of the absorbed photons multiplied by the average number of excited electrons per a single absorbed photon, which is about 422 at $t = 30$ fs. In the present model, we do not take into account the electron diffusion for electrons with energies below the lowest ionization threshold (11.26 eV for diamond), i.e., we assume that such electrons completely stop their motion (see the justification in the previous section).

Similarly as in Fig. 1, in Fig. 2 one can see the increasing effect of the ballistic electron transport on the spatial redistribution of absorbed energy when decreasing the beam spot size. The curves show that for tight focusing conditions (with the focus size smaller or comparable to the electron range), the electron spread caused by ballistic electrons significantly reduces the peak electron density, also affecting wing regions.

The resulting effective distribution of the absorbed x-ray dose determines the probability of diamond graphitization.

V. DISCUSSION

According to our earlier simulations with two hybrid codes XTANT (relying on transferable tight binding description of solid's band structure) [14,22] and XTANT+ (relying on density functional tight binding of the band structure) [20], diamond undergoes ultrafast graphitization when the number of excited electrons in the conduction band reaches about 2.14% or 4.60%, respectively. This value corresponds to the ratio of the number of excited electrons to the initial number of valence electrons, which is four per atom in diamond. Note that the XCASCADE-3D model applied in this work is based on the atomistic approximation and does not include the electron-hole recombination or equilibration [12]. However, these effects should not play a significant role on the considered ultrafast timescales, up to 30 fs.

The simulation results presented in the previous section show that the considered experimental conditions lead to the peak electron densities presented in the last column of Table I. One can conclude that the conditions achieved in cases (3.1) and (3.2) correspond to the case of ultrafast amorphization [20], with the peak dose too high for the graphitization to occur. According to our XTANT+ calculations [20], the amorphization threshold for electron density lies between 12% to 16%. In contrast, in cases (1.1)–(1.4) the peak electron density is too low to expect any graphitization.
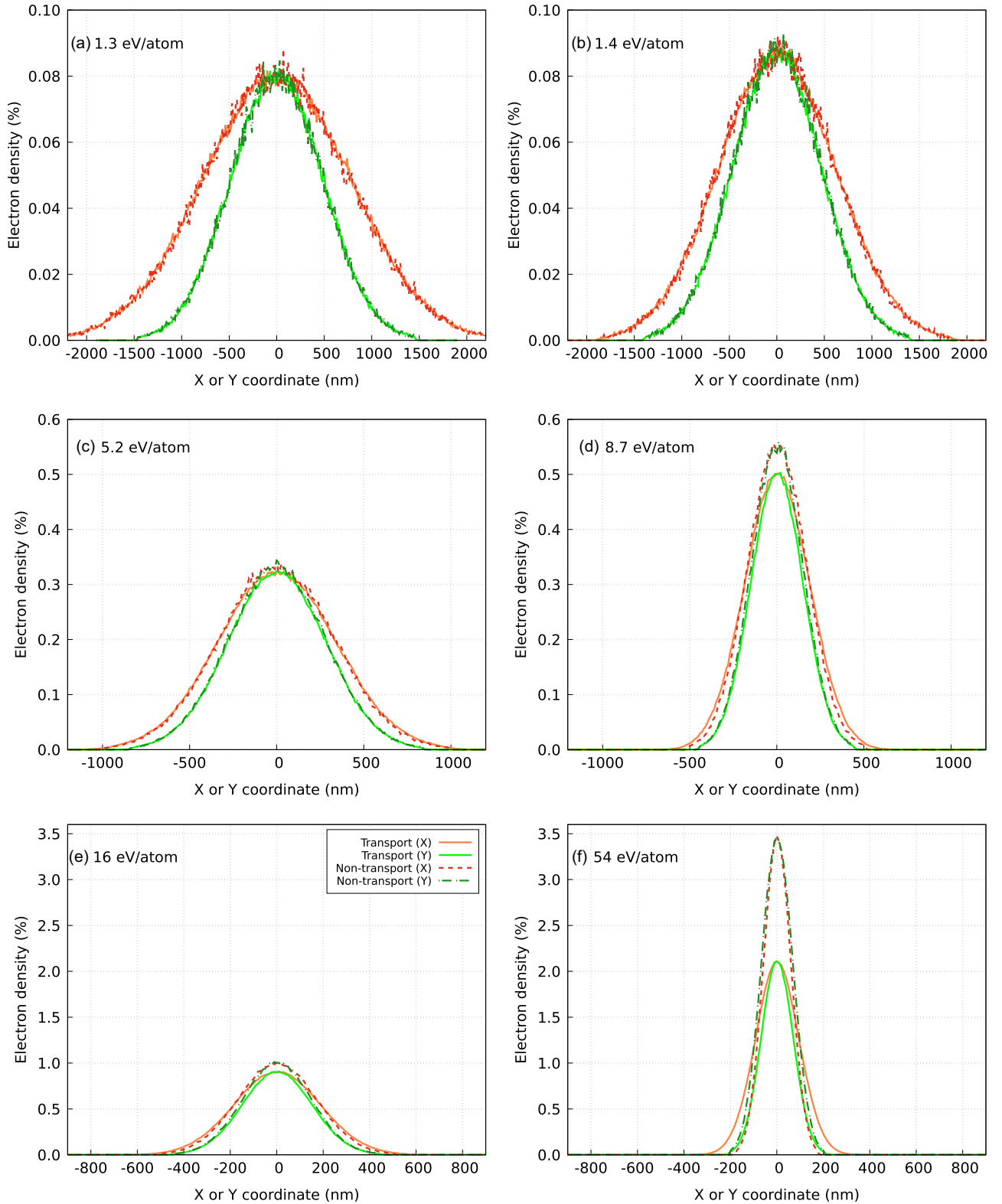
FIG. 1. Results of XCASCADE-3D simulations for diamond irradiated with an 6 fs x-ray pulse (photon energy of 7 keV). The solid lines represent the electron density at time $t = 0$ fs (i.e., at the temporal maximum of the pulse intensity) for the absorbed doses of (a) 1.3, (b) 1.4, (c) 5.2, (d) 8.7, (e) 16, and (f) 54 eV/atom. Red color corresponds to the direction along the polarization axis x (with $Y = 0$), while green color corresponds to the perpendicular direction (with $X = 0$). The dashed and dash-dotted lines represent the respective x and y electron densities estimated in nontransport cases, i.e., they essentially correspond to the x-ray spatial profiles.
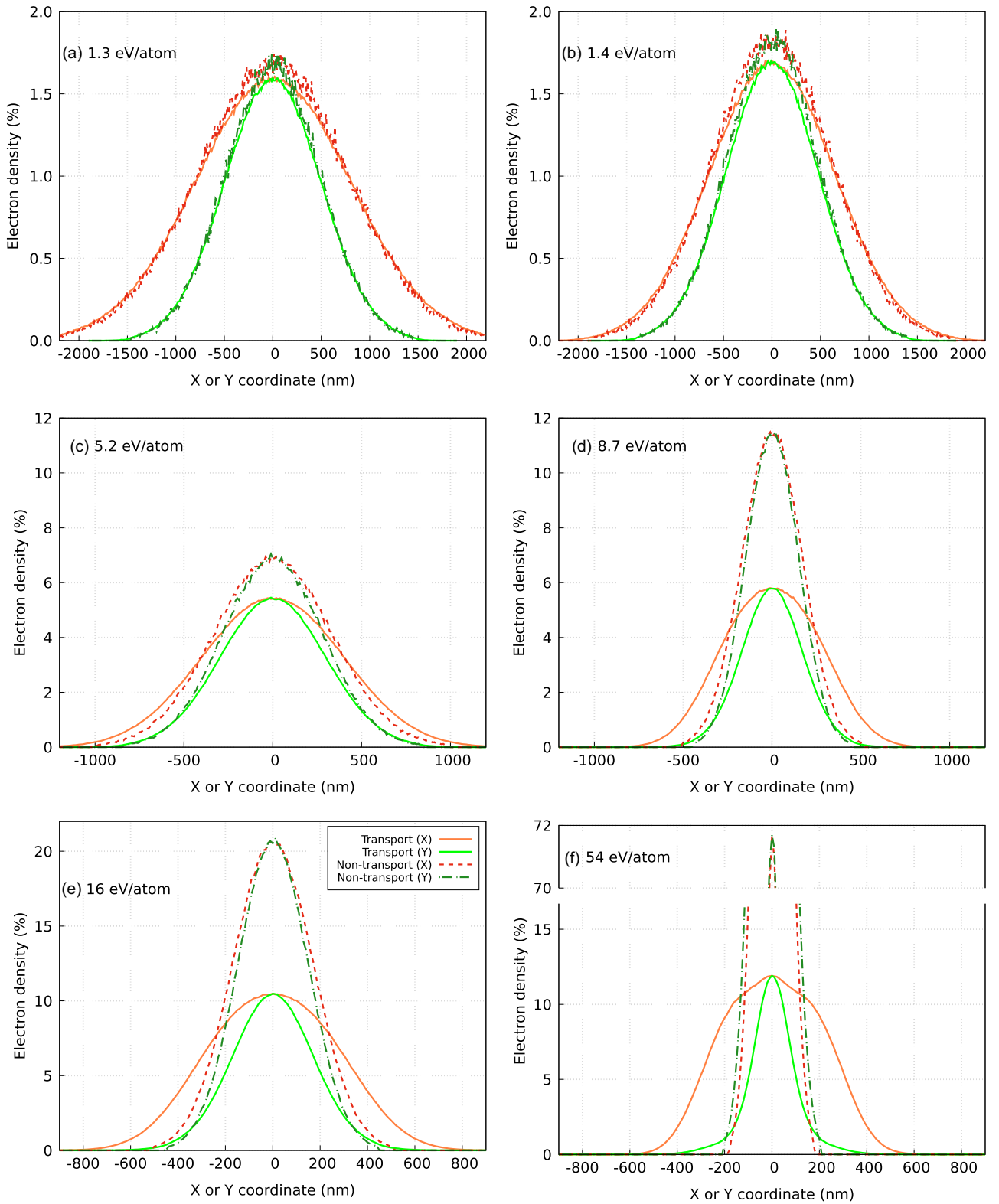
FIG. 2. Calculated electron density at time $t = 30$ fs (i.e., after the cascading has finished). The other parameters and observables are the same as in Fig. 1.

In cases (2.1)–(2.3), the predictions of the two hybrid codes differ. XTANT predictions indicate that even in these cases the electron densities were too high to achieve the graphitization, while XTANT+ predictions suggest that the partial graphitization could be possible in the near-peak region on the

timescale of about 500 fs. In Ref. [8], the signal was too weak to observe such partial graphitization on the experimentally accessible ultrafast time scale (up to 300 fs).

Cases (3.1), (3.2), or (2.1)–(2.3) might result in graphitization regions located in the wing region of the pulse, and

further apart, although a possible heat transfer from the peak to the wings could hinder the graphitization process.

One of the limitations of the XCASCADE-3D model is that it relies on the assumption of the independent electron cascades. This assumption is valid when the density of *cascading* electrons is considerably lower than the atomic density, i.e., at least ten times smaller than the atomic density. The condition also justifies the usage of cross sections for unexcited materials in the code. We have checked the validity of the above condition for the cases presented in Figs. 1 and 2, i.e., when the cascading process was still ongoing or when it finished, respectively. The plots represent the normalized density of excited electrons (the ratio of the number of excited electrons to the number of valence electrons which is here four per atom). Therefore, the limiting electron density value is 2.5%. This is the case for all plots in Figs. 1, 2(a), and 2(b). However in Figs. 2(c)–2(f), the electron density increases above this limit, i.e., the XCASCADE-3D predictions should be treated only as indicative. In any case, the obtained prediction span confirms a need of the careful consideration of each specific dose case at the stage of experimental planning.

In summary, triggering graphitization or other phase transitions by hard x-ray photons is difficult due to the escape of electrons from the beam focus. The decisive parameter here is the electron range, i.e., how it compares to the focal beam size. In the hard x-ray regime discussed above, the released photo and Auger electrons can be very energetic, e.g., for 7 keV photons the photoelectron range amounts to 312 nm. In case of submicrometer focusing, such electrons can strongly influence redistribution of the x-ray absorbed dose deposited in various lateral regions of the crystal. In contrast, in case of soft x-ray induced ultrafast graphitization, indirectly observed in [14], the electron range was only $\sim$0.8 nm vs micrometer beam focus, i.e., the absorbed x-ray energy was not carried out by the electrons out of the beam focus in this case.

Therefore, for future experiments on x-ray induced phase transitions, dedicated simulations are necessary for establishing optimal experimental conditions ensuring a required dose distribution.

[1] W. Ackermann, G. Asova, V. Ayvazyan, A. Azima, N. Baboi, J. Bähr, V. Balandin, B. Beutner, A. Brandt, A. Bolzmann *et al.*, Operation of a free-electron laser from the extreme ultraviolet to the water window, Nat. Photonics **1**, 336 (2007).

[2] E. Allaria, R. Appio, L. Badano, W. Barletta, S. Bassanese, S. Biedron, A. Borga, E. Busetto, D. Castronovo, P. Cinquegrana *et al.*, Highly coherent and stable pulses from the FERMI seeded free-electron laser in the extreme ultraviolet, Nat. Photonics **6**, 699 (2012).

[3] P. Emma, R. Akre, J. Arthur, R. Bionta, C. Bostedt, J. Bozek, A. Brachmann, P. Bucksbaum, R. Coffee, F.-J. Decker *et al.*, First lasing and operation of an ångstrom-wavelength free-electron laser, Nat. Photonics **4**, 641 (2010).

[4] T. Ishikawa, H. Aoyagi, T. Asaka, Y. Asano, N. Azumi, T. Bizen, H. Ego, K. Fukami, T. Fukui, Y. Furukawa *et al.*, A compact X-ray free-electron laser emitting in the sub-ångström region, Nat. Photonics **6**, 540 (2012).

[5] H. Weise and W. Decking, Commissioning and first lasing of the European XFEL, Proc. FEL'17, 9 (2017).

[6] J. Gaudin, N. Medvedev, J. Chalupský, T. Burian, S. Dastjani-Farahani, V. Hájková, M. Harmand, H. O. Jeschke, L. Juha *et al.*, Photon energy dependence of graphitization threshold for diamond irradiated with an intense XUV FEL pulse, Phys. Rev. B **88**, 060101(R) (2013).

[7] I. Inoue, Y. Inubushi, T. Sato, K. Tono, T. Katayama, T. Kameshima, K. Ogawa, T. Togashi, S. Owada, Y. Amemiya, T. Tanaka, T. Hara, and M. Yabashi, Observation of femtosecond X-ray interactions with matter using an X-ray–X-ray pump–probe scheme, Proc. Natl. Acad. Sci. USA **113**, 1492 (2016).

[8] P. Heimann, N. J. Hartley, I. Inoue, V. Tkachenko, A. Antoine, F. Dorchies, R. Falcone, J. Gaudin, H. Höppner *et al.*, Non-thermal structural transformation of diamond driven by x-rays, Struct. Dyn. **10**, 054502 (2023).

[9] B. Ziaja, D. van der Spoel, A. Szöke, and J. Hajdu, Auger-electron cascades in diamond and amorphous carbon, Phys. Rev. B **64**, 214104 (2001).

[10] R. Follath, T. Koyama, V. Lipp, N. Medvedev, K. Tono, H. Ohashi, L. Patthey, M. Yabashi, and B. Ziaja, X-ray induced damage of B_4C-coated bilayer materials under various irradiation conditions, Sci. Rep. **9**, 2029 (2019).

[11] N. Medvedev, Femtosecond X-ray induced electron kinetics in dielectrics: Application for FEL-pulse-duration monitor, Appl. Phys. B **118**, 417 (2015).

[12] V. Lipp, I. Milov, and N. Medvedev, Quantifying electron cascade size in various irradiated materials for free-electron laser applications, J. Synchrotron Radiat. **29**, 323 (2022).

[13] P. Heimann, I. Inoue, F. Dorchies, R. Falcone, J. Gaudin, H. Hoeppner, H. J. Lee, V. Lipp, P. Martinez, N. Medvedev *et al.*, Characterization of the non-thermal phase transitions of diamond and silicon with two-color X-ray pulses, SPring-8/SACLA Res. Rep. **11**, 435 (2023).

[14] F. Tavella, H. Höppner, V. Tkachenko, N. Medvedev, F. Capotondi, T. Golz, Y. Kai, M. Manfredda, E. Pedersoli, M. J. Prandolini *et al.*, Soft x-ray induced femtosecond solid-to-solid phase transition, High Energy Density Phys. **24**, 22 (2017).

[15] P. L. Silvestrelli, A. Alavi, M. Parrinello, and D. Frenkel, *Ab initio* molecular dynamics simulation of laser melting of silicon, Phys. Rev. Lett. **77**, 3149 (1996).

[16] S. I. Kudryashov and V. I. Emel'yanov, Band gap collapse and ultrafast "cold" melting of silicon during femtosecond laser pulse, JETP Lett. **73**, 228 (2001).

[17] A. Rousse, C. Rischel, S. Fourmaux, I. Uschmann, S. Sebban, G. Grillon, P. Balcou, E. Förster, J. P. Geindre, P. Audebert *et al.*, Non-thermal melting in semiconductors measured at femtosecond resolution, Nature (London) **410**, 65 (2001).

[18] M. Harb, R. Ernstorfer, C. T. Hebeisen, G. Sciaini, W. Peng, T. Dartigalongue, M. A. Eriksson, M. G. Lagally, S. G. Kruglik, and R. J. D. Miller, Electronically driven structure changes of Si captured by femtosecond electron diffraction, Phys. Rev. Lett. **100**, 155504 (2008).

[19] N. Medvedev, H. Jeschke, and B. Ziaja, Nonthermal phase transitions in semiconductors induced by a femtosecond extreme ultraviolet laser pulse, New J. Phys. **15**, 015016 (2013).

[20] V. Lipp, V. Tkachenko, M. Stransky, B. Aradi, T. Frauenheim, and B. Ziaja, Density functional tight binding approach utilized to study X-ray-induced transitions in solid materials, Sci. Rep. **12**, 1551 (2022).

[21] J. Lütgert, P. Hesselbach, M. Schörner, V. Bagnoud, R. Belikov, P. Drechsel, B. Heuser, O. S. Humphries, P. Katrik, B. Lindqvist *et al.*, Temperature and structure measurements of heavy-ion-heated diamond using in situ X-ray diagnostics, Matter Radiat. Extremes **9**, 047802 (2024).

[22] Medvedev, Nikita, Tkachenko, Viktor, Lipp, Vladimir, Li, Zheng, and Ziaja Beata, Various damage mechanisms in carbon and silicon materials under femtosecond X-ray irradiation, 4open **1**, 3 (2018).

[23] H. Yumoto, H. Mimura, T. Koyama, S. Matsuyama, K. Tono, T. Togashi, Y. Inubushi, T. Sato, T. Tanaka, T. Kimura *et al.*, Focusing of X-ray free-electron laser pulses with reflective optics, Nat. Photonics **7**, 43 (2013).

[24] H. Mimura, H. Yumoto, S. Matsuyama, T. Koyama, K. Tono, Y. Inubushi, T. Togashi, T. Sato, J. Kim, R. Fukui *et al.*, Generation of 10^{20} W cm^{-2} hard X-ray laser pulses with two-stage reflective focusing system, Nat. Commun. **5**, 3539 (2014).

[25] H. Yumoto, Y. Inubushi, T. Osaka, I. Inoue, T. Koyama, K. Tono, M. Yabashi, and H. Ohashi, Nanofocusing optics for an X-ray free-electron laser generating an extreme intensity of 100 EW/cm^2 using total reflection mirrors, Appl. Sci. **10**, 2611 (2020).

[26] J. Yamada, S. Matsuyama, I. Inoue, T. Osaka, T. Inoue, N. Nakamura, Y. Tanaka, Y. Inubushi, T. Yabuuchi, K. Tono *et al.*, Extreme focusing of hard X-ray free-electron laser pulses enables 7 nm focus width and 10^{22} W cm^{-2} intensity, Nat. Photon. **18**, 685 (2024).

[27] V. Lipp, B. Ziaja-Motyka, and N. Medvedev, XCASCADE (3D) (2023), doi:10.5281/zenodo.8204314.

[28] V. Lipp, N. Medvedev, and B. Ziaja, Classical Monte-Carlo simulations of X-ray induced electron cascades in various materials, in *Damage to VUV, EUV, and X-Ray Optics VI*, Vol. 10236, edited by R. S. L Juha, and S Bajt, International Society for Optics and Photonics (SPIE, 2017), pp. 40–48.

[29] I. Milov, V. Lipp, D. Ilnitsky, N. Medvedev, K. Migdal, V. Zhakhovsky, V. Khokhlov, Y. Petrov, N. Inogamov, S. Semin *et al.*, Similarity in ruthenium damage induced by photons with different energies: From visible light to hard X-rays, Appl. Surf. Sci. **501**, 143973 (2020).

[30] V. Tkachenko, V. Lipp, M. Büscher, F. Capotondi, H. Höppner, N. Medvedev, E. Pedersoli, M. J. Prandolini, G. M. Rossi *et al.*, Effect of Auger recombination on transient optical properties in XUV and soft X-ray irradiated silicon nitride, Sci. Rep. **11**, 5203 (2021).

[31] D. E. Cullen, A survey of atomic binding energies for use in EPICS2017, *Nuclear Data Section, International Atomic Energy Agency* (Vienna, Austria, 2018).

[32] O. Keski-Rahkonen and M. O. Krause, Total and partial atomic-level widths, At. Data Nucl. Data Tables **14**, 139 (1974).

[33] V. T. Davis, Classical model of photoelectron angular distributions, in *Introduction to Photoelectron Angular Distributions: Theory and Applications* (Springer International Publishing, Cham, 2022), pp. 61–76.

[34] B. Henke, E. Gullikson, and J. Davis, X-ray interactions: Photoabsorption, scattering, transmission, and reflection at $E = $ 50-30000 eV, $Z = $ 1-92, At. Data Nucl. Data Tables **54**, 181 (1993).